(12)

SIGNAL/NOISE RATIO OF HOLOGRAPHIC IMAGES

W. J. Burke

RCA LABORATORIES
Princeton, New Jersey 08540

OCTOBER 1975

FINAL REPORT
(June 24, 1975 to September 23, 1975)

Prepared for:
NAVAL AIR SYSTEMS COMMAND
DEPARTMENT OF THE NAVY
Washington, D.C. 20361

Contract No. N00019-75-M-0494

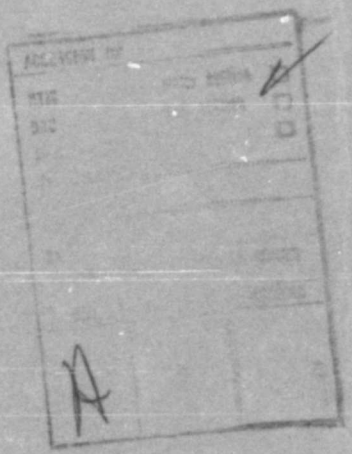

UNCLASSIFIED

SECURITY CLASSIFICATION OF THIS PAGE (When Data Entered)

REPORT DOCUMENTATION PAGE	READ INSTRUCTIONS BEFORE COMPLETING FORM
1. REPORT NUMBER	2. GOVT ACCESSION NO. 3. RECIPIENT'S CATALOG NUMBER
4. TITLE (and Subtitle) SIGNAL/NOISE RATIO OF HOLOGRAPHIC IMAGES	5. TYPE OF REPORT & PERIOD COVERED Final Report, 24 Jun - 23 Sep 75 (6-24-75 to 9-23-75)
	6. PERFORMING ORG. REPORT NUMBER PRRL-75-CR-66
7. AUTHOR(s) W. J. Burke	8. CONTRACT OR GRANT NUMBER(s) N00019-75-M-0494
9. PERFORMING ORGANIZATION NAME AND ADDRESS RCA Laboratories Princeton, NJ 08540	10. PROGRAM ELEMENT, PROJECT, TASK AREA & WORK UNIT NUMBERS
11. CONTROLLING OFFICE NAME AND ADDRESS Naval Air Systems Command Department of the Navy Washington, D.C. 20361	12. REPORT DATE October 1975
	13. NUMBER OF PAGES 33 (12) 33p.
14. MONITORING AGENCY NAME & ADDRESS (if different from Controlling Office)	15. SECURITY CLASS. (of this report) Unclassified
	15a. DECLASSIFICATION/DOWNGRADING SCHEDULE N/A

16. DISTRIBUTION STATEMENT (of this Report)

APPROVED FOR PUBLIC RELEASE;
DISTRIBUTION UNLIMITED

17. DISTRIBUTION STATEMENT (of the abstract entered in Block 20, if different from Report)

DDC RECEIVED DEC 31 1975 A

18. SUPPLEMENTARY NOTES

19. KEY WORDS (Continue on reverse side if necessary and identify by block number)

Holography, Volume Holography, Holographic Storage, Holographic Fixing, Iron-doped $LiNbO_3$, Holographic Signal/Noise

20. ABSTRACT (Continue on reverse side if necessary and identify by block number)

This report describes the results of the currently obtainable signal/noise (S/N) ratio of images readout from thick phase holograms stored in iron-doped $LiNbO_3$. Using multiple object beam illumination an S/N ratio of ~27 dB was measured for a white field. No significant decrease in the measured S/N ratio was observed with the increasing number of holograms stored.

DD FORM 1 JAN 73 1473

UNCLASSIFIED

SECURITY CLASSIFICATION OF THIS PAGE (When Data Entered)

299 000

20.

PREFACE

This Final Report describes research performed under Contract No. N00019-75-M-0494 of RCA Laboratories in the Communications Research Laboratory, K. Powers, Director. It describes work done from June 24, 1975 to September 23, 1975. The Project Supervisor is B. Williams and the Principal Investigator was W. J. Burke.

TABLE OF CONTENTS

Section		Page
I.	INTRODUCTION.	1
II.	MEASUREMENT TECHNIQUES	4
	A. Storage Medium.	4
	B. Diffraction Efficiency.	4
	C. Recording Apparatus	4
	D. Noise Measurements.	5
	E. Definition of Noise	8
III.	S/N MEASUREMENTS	10
	A. Transmitted Object Beam	10
	B. Readout Images.	15
	1. Crosstalk	15
	2. Hologram Amplitude.	15
	3. S/N Measurements with the Image Slicer.	16
	4. S/N Measurement with Scanning Photomultiplier	16
	5. Noise Measurements with a Spectrum Analyzer	20
IV.	SUMMARY AND CONCLUSIONS	25
	REFERENCES.	26

LIST OF ILLUSTRATIONS

Figure		Page
1.	Schematic diagram of recording and readout optical system.	5
2.	Photograph of white field portion of object transparency	6
3.	Schematic diagram on noise measurement system using image slicer .	7
4.	Schematic diagram of scanning photomultiplier system	8
5.	Waveform monitor oscilloscope tracing of a single TV line of the image of the 100th hologram recorded and fixed. The signal has a side-to-side rolloff due to nonuniformity of the recording light beams.	9
6.	Television image of the object transparency (a) illuminated with a single laser beam; (b) illuminated with a tungsten filament lamp	11
7.	Television image of the object transparency illuminated with multiple laser beams	12
8.	Spectrum analyzer tracing of the frequency spectrum of the readout image in showing 6 MHz frequency component due to the phase grating.	13
9.	(a) Television image of the object transparency as in Fig. 7, but with 2.5X greater magnification in the recording optics. (b) Spectrum analyzer tracing of the frequency spectrum of the image shown in (a). The grating frequency and its harmonics are reduced by a factor of 2 corresponding to the increased system magnification.	14
10.	Television image of the (a) 1st; (b) 50th, and (c) 100th hologram recorded and fixed.	17
11.	S/N ratio as a function of hologram number measured with the image slicer	18
12.	S/N ratio as a function of spatial frequency of the image readout from a recorded and fixed multibeam hologram measured with the scanning photomultiplier and of the object transparency illuminated with a single laser beam. The optical magnification is 8X that in Fig. 11.	19
13.	Spectrum analyzer tracing at an optical magnification 2X that of Fig. 11 of the readout image from the 1st of 100 holograms. (a) over the 0 to 5 MHz frequency range; (b) over the 0 to 10 MHz frequency range.	21
14.	Spectrum analyzer tracing as in Fig. 13 of the readout image from the 100th hologram over the 0 to 5 MHz frequency range	22

LIST OF ILLUSTRATIONS (Continued)

Figure		Page
15.	Spectrum analyzer tracing of the object transparency illuminated with a single laser beam. (a) over the frequency range 0 to 5 MHz; (b) 0 to 10 MHz	23
16.	Data from Fig. 13 and Fig. 15 plotted as a function of spatial frequency. The optical magnification is 1/4 that shown in Fig. 12.	24

I. INTRODUCTION

Volume phase holography is a technique for the storage of graphic or binary information in holographic form throughout the entire volume of a thick (~1 cm) storage medium. Volume holograms have an angular selectivity on readout of the stored information, i.e., the angle of the readout beam must satisfy the Bragg condition for constructive interference. Using this approach, many different holograms can be stored in the same volume since the angular bandwidth of a given hologram decreases with the increasing thickness of the storage medium. Thus, as the thickness increases the number of separable angular positions increases, with the number of such angular positions being proportional to the ratio of medium thickness to the spacing of the holographic grating (~1 μm). The advantages of this approach are several:

(1) Using phase holograms, diffraction efficiencies approaching 100% are possible.

(2) Using thick storage media, large numbers of holograms can be stored in the same volume.

(3) Simplicity of access, since only the readout beam angle must be changed.

The applicability of this technique has been limited until recently by the availability of storage media with the desired recording properties. In the last several years, however, iron-doped $LiNbO_3$ has been developed at RCA Laboratories as a thick phase holographic storage medium. During this period we have developed techniques for the growth and sensitization of $LiNbO_3$ and an understanding of the recording and fixing mechanism. Phase holograms are recorded in iron-doped $LiNbO_3$ by photoexcitation of electrons trapped at Fe^{3+} sites with subsequent drift or diffusion of the electrons from regions of high light intensity in the interference pattern of the light beams into regions of lower light intensity and retrapping at Fe^{3+} ions. Through this process a trapped electronic space charge pattern is formed which mirrors the original light intensity pattern. This space charge pattern modulates the index of refraction through the electro-optic effect producing the phase grating [1-4].

1. J. J. Amodei, W. Phillips, and D. L. Staebler, IEEE J. Quantum Electron. QE-7, 63 (1971).
2. G. E. Peterson, A. M. Glass, and T. J. Negran, Appl. Phys. Lett. 19, 130 (1971).
3. F. S. Chen, J. T. LaMacchia, and D. B. Frazer, Appl. Phys. Lett. 13, 233 (1968).
4. D. L. Staebler and J. J. Amodei, J. Appl. Phys. 43, 1042 (1972).

Heating the crystal in which the hologram is stored to between 100° and 200°C produces a transport of an ionic species which neutralizes the electronic space charge pattern [5]. Upon cooling to room temperature and redistributing the electronic space charge pattern with incoherent light, a hologram due to the ionic space charge pattern remains.

Using these techniques we have stored more than 500 holograms, each hologram having a diffraction efficiency greater than 2.5%. Two recent developments have opened up the possibility of further improvement of these results:

(1) Theoretical calculations have shown that the erase/record asymmetry increases with increasing Fe^{3+}/Fe^{2+} ratio. Thus, the erasure of holograms during sequential recording can be reduced [6].

(2) Silicon has been identified as a mobile ion in iron-doped $LiNbO_3$. If silicon is, in fact, the mobile fixing ion, then an increase in the silicon concentration could lead to lower fixing temperatures, thus reducing the thermal erasure during recording [6].

Because of these results, together with the high optical quality of $LiNbO_3$ crystals, and our investigation of other dopants in $LiNbO_3$ and other host materials, we have concluded that iron-doped $LiNbO_3$ is the optimum volume phase storage medium at present.

In practice, the theoretical capability for high density storage is limited by the required Signal/Noise (S/N) ratio in the image readout from the stored hologram. There are several different sources of noise in images stored as thick phase holograms.

(a) Intermodulation distortion which results from gratings recorded by interference between different parts of the object beam. In thick phase holograms this appears as an image readout off the Bragg angle for the reconstruction of the hologram.

(b) Crosstalk between holograms stored in the same volume, which results from using too small an angular separation between holograms.

(c) Statistical noise arising from fluctuations in the number of electrons or mobile ions which form the holographic grating.

---

5. J. J. Amodei and D. L. Staebler, Appl. Phys. Lett. 18, 540 (1971).
6. W. J. Burke, W. Phillips, D. L. Staebler, and B. F. Williams, *Materials for Phase Holographic Storage*, Final Report, Contract No. N00019-74-C-0312, April 1975.

(d) Cosmetic noise which is due to scattering of light from imperfections in the object transparency, the recording medium, or the recording and readout optics. This effect is particularly prominent in holographic storage due to the monochromatic nature of the recording light.

(e) Optical damage of the storage medium during recording or readout. This damage occurs by the same mechanism by which the hologram itself is recorded, a hologram of the interference of the recording or readout beam with themselves when a portion of the beams undergo scattering. During recording, this damage is recorded and fixed concurrently with the hologram of interest. This effect is strongly suppressed using the record-while-hot technique discussed above. The reason for this suppression appears to be that the optical damage grows nonlinearly with the electronic space charge field due to scattering, and this space charge field is continually compensated by the mobile ions [7]. In readout, the optical damage is not fixed and can be erased using incoherent light.

An experimental determination of the S/N ratio has been made, and is discussed in this report. The purpose of this program is to measure the composite S/N ratio in the readout image from holograms stored in iron-doped $LiNbO_3$ using our currently existing recording apparatus. We have measured the S/N ratio in images from crystals in which 10 and 100 holograms have been recorded and fixed.

The remainder of this report is organized into three sections covering the measurement techniques, S/N measurements on the fixed holograms, and the conclusions drawn from these results.

---

7. G. A. Alphonse and W. Phillips, *Read-Write Holographic Memory with Iron-Doped $LiNbO_3$*, Final Report, Contract No. NAS8-26808, May 1975.

II. MEASUREMENT TECHNIQUES

A. STORAGE MEDIUM

Poled single crystals of $LiNbO_3$ containing 0.01 to 0.05 mole % iron were used in these studies. The crystals were oxidized in an Ar + O_2 atmosphere at 950°C for 24 hours to obtain the desired optical density (0.2 to 0.3 at 4880 Å). The oxygen content of the atmosphere is varied depending on iron concentration and crystal thickness [8]. After this treatment, the crystals were repolished using a SYTON chemical polish to reduce surface scattering. The crystals were then anti-reflection-coated with a single layer of SiO_2, 825 Å thick, by D. Hoffman of RCA Laboratories. In the results reported here, 0.4- and 0.5-cm-thick crystals were used.

B. DIFFRACTION EFFICIENCY

The holograms studied were recorded and fixed so that each hologram had a diffraction efficiency ranging from 7.5% to 10%. To achieve this range of diffraction efficiencies for all holograms, the holograms were sequentially recorded with successively smaller exposures to compensate for optical and thermal erasure [9]. The range of final, fixed diffraction efficiencies is due to a lack of perfect compensation of the erasure and fluctuations in the recording conditions (laser power variation, crystal vibration, etc.).

C. RECORDING APPARATUS

Holograms were recorded using an Ar^+ ion laser operating in a TEM_o mode at 4880 Å. A schematic diagram of the recording apparatus is shown in Fig. 1. Beam expanders with spatial filters are used in both beams to reduce or remove nonuniformities in the beams due to light scattering and multiple reflections in the preceding portions of the optical system.

---

8. D. L. Staebler, W. Phillips, W. Burke, and B. W. Faughnan, *Materials for Phase Holographic Storage*, Final Report, Contract No. N00019-73-C-0273, February 1974.
9. W. J. Burke and D. L. Staebler, *Volume Hologram Material Device Feasibility*, Final Report, Contract No. N62269-72-C-0793, June 1973.

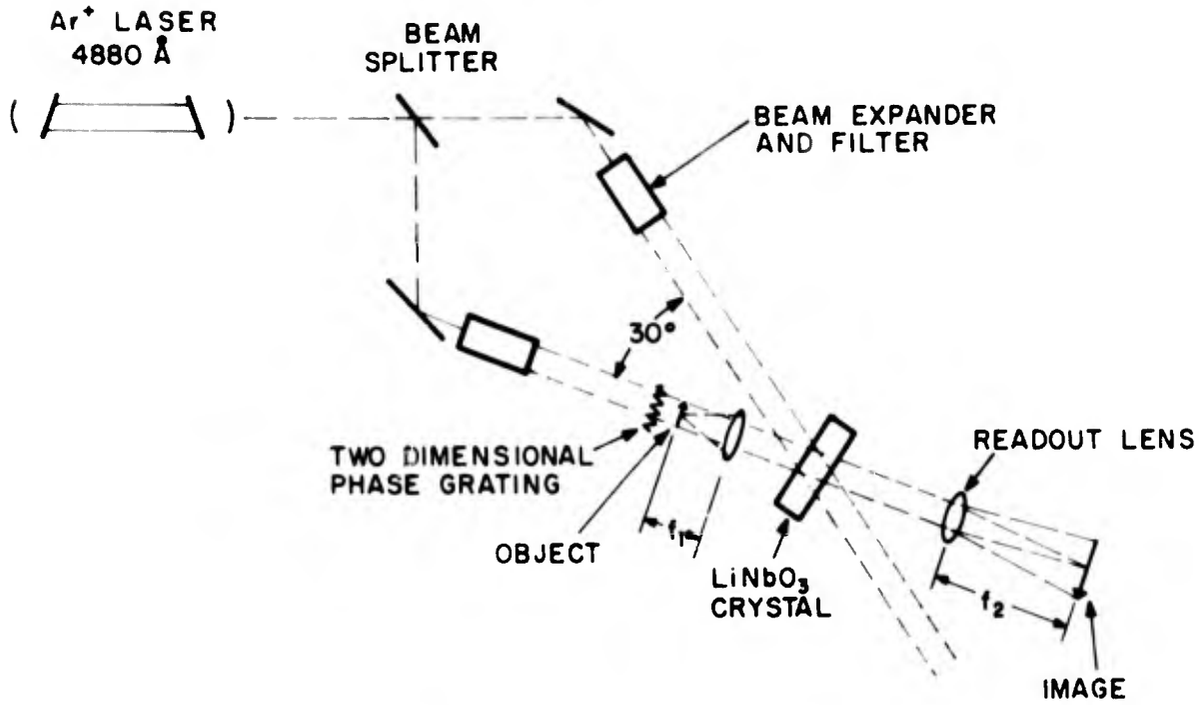

Figure 1. Schematic diagram of recording and readout optical system.

The object to be recorded was a 16-mm transparency of a uniform field on a black background as shown in Fig. 2. The two slits were used for focusing of the object. This particular object was chosen for these measurements because the large white area provides a worst case for image uniformity and appearance.

Fraunhofer holograms of the object were recorded primarily for simplicity in varying the readout geometry. For this case the object is located at the front focal plane of the first lens. Light from a given point at the object is then focused using the second lens. Then the magnification of the readout image is simply the ratio of the readout imaging lens to the recording lens. We used magnifications of 1.25, 2.5, and 10, depending upon the particular type of measurement.

D. NOISE MEASUREMENTS

For readout of the stored holograms, three different systems were used. The first used a GPL1000 television camera for detection of the image and display on a Conrac CZB17 monitor. The second system used direct projection of

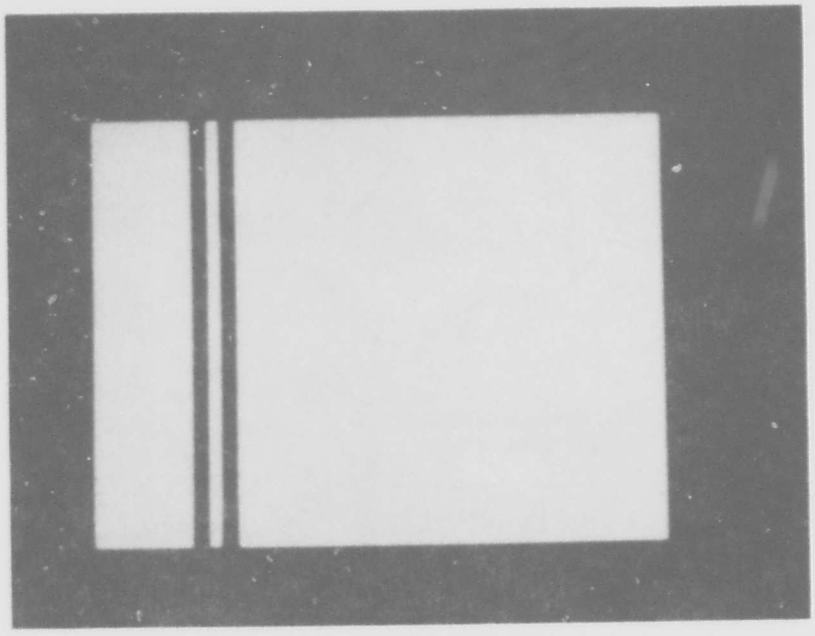

Figure 2. Photograph of white field portion of object transparency.

the image with an RCA 931A photomultiplier tube for detection of the signal. The third system was a Hewlett-Packard 8553B spectrum analyzer.

A block diagram of the apparatus used for the noise measurements with the television readout apparatus is shown in Fig. 3. The detected image magnified 1.25 times is viewed first on a Tektronix model 529 waveform monitor on which single or multiple lines or fields can be displayed. The TV signal is then fed to an RCA-developed image slicer,* and then to the Conrac monitor. The signal can either bypass the image slicer for direct viewing on the monitor or be processed by the slicer, and the result displayed on the monitor.

In the image slicer, the ac-coupled video signal is added to a dc voltage controlled by a helipot. The sum is fed to a nonlinear circuit whose voltage transfer function is a negative going pulse of approximately Gaussian shape, 0.7 V in output amplitude, and about 0.014 V wide at the 50% points. When the output of this device is fed to the monitor, all portions of the video signal which fall within $\pm$0.007 V of the voltage set by the helipot appear as white areas on the screen. When the dc level set corresponds to blanking level, the device puts out a 0.7 V blanking waveform which causes the entire monitor screen

*E. C. Fox, private communication.

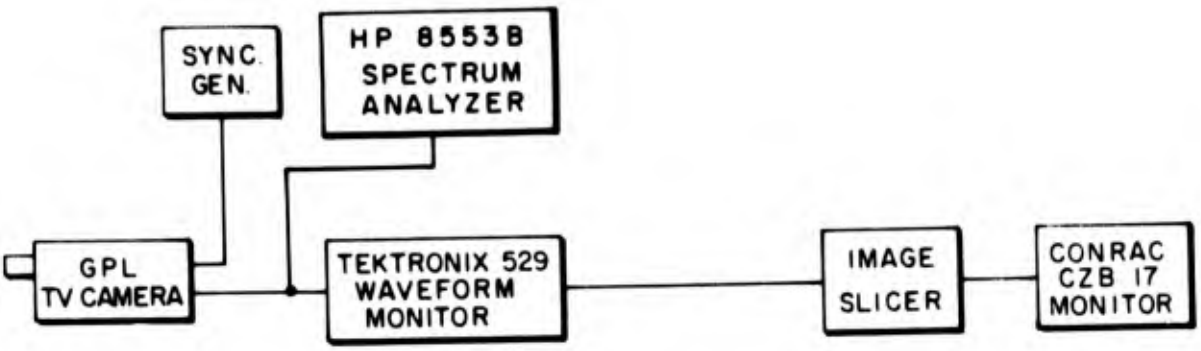

Figure 3. Schematic diagram on noise measurement system using image slicer.

to suddenly increase in brightness. Noise was measured on a peak-to-peak basis, by adjusting the dc level in the slicer to the two levels at which just a few white dots, representing the noise peaks, appeared in the area in question. The difference of these levels was taken as the peak-to-peak noise.

A block diagram of the scanning photomultiplier apparatus used to measure the noise in direct projection is shown in Fig. 4. A motor-driven RCA 931A photomultiplier tube with pinhole apertures of varying sizes was used to scan a line across the image. The output was then displayed on a Y,T recorder. The maximum spatial frequency response of this system was calculated in the following way: we assume that the required time of observation of an element of the image is equal to the time constant T_o of the detection apparatus which is $T_o = 0.13$ s in this case. During this time interval the aperture of the photomultiplier samples a length $X_m = vT_o$, where v is the scan velocity. X_m is, then, the smallest element which can be sampled. The smallest velocity obtainable with our apparatus is $\sim$250 μm/s which gives $X_m = 32.5$ μm. The corresponding maximum spatial frequency is 30.8 mm^{-1}. The system response can be decreased by increasing the scan velocity of the time constant, or by increasing the pinhole size. The effective response of the system can also be increased by magnification of the image. For the scanning photomultiplier measurements the magnification was 10X.

The spectrum analyzer was used to measure the output in frequency of the television camera pickup of the image. This system scans the input video signal with a narrow (in this case, 10 kHz or 30 kHz) bandpass filter and displays the video signal spectrum as a function of frequency. This method of

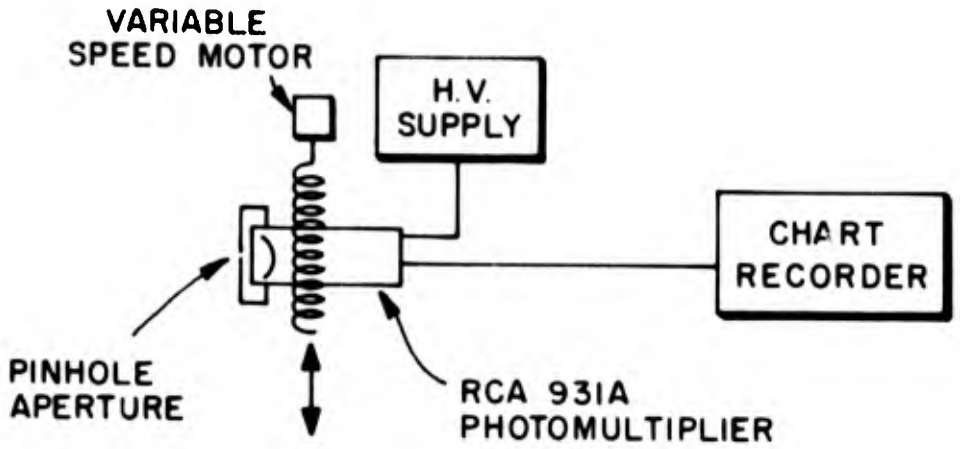

Figure 4. Schematic diagram of scanning photomultiplier system.

measurement differs from the TV and scanning photomultiplier methods in that these systems measure the signal/integrated noise up to a given frequency while the spectrum analyzer provides a measure of the video signal plus noise at the particular frequency. The output of the spectrum analyzer is then the derivative of the signal/integrated noise measured with the TV and photomultiplier systems. The image was magnified 2.5X for these measurements.

E. DEFINITION OF NOISE

In the measurements reported here image noise is defined as the spatial variation in the intensity of the readout image. We do not include as a noise source the fluctuation in intensity from image to image, since it is assumed that such fluctuations can be corrected either with improved recording apparatus or by gain control in the readout optics (e.g., variation in readout laser power). We have also excluded as a noise source variations in uniformity across the image which arise from the fact that the holograms were recorded using Gaussian beams 1.9 to 2.5 cm in diameter. In this work the radial variation in intensity, primarily of the reference beam, over the distance for which the object and reference beams overlapped, produced a 35 to 40% variation in the uniformity of the diffraction efficiency. This variation is a smooth continuous one with higher frequency noise superimposed as shown in Fig. 5. Figure 5 is an oscilloscope tracing of a single horizontal line of the image as detected with the television camera and the Tektronix model 529 waveform monitor. The variation in the signal amplitude is a measure of the

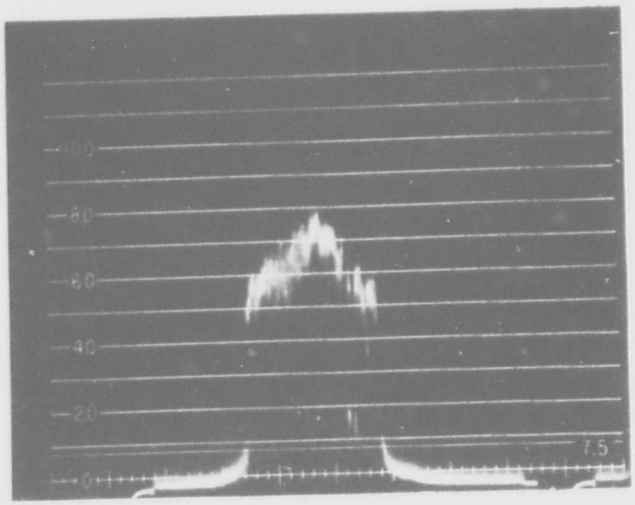

Figure 5. Waveform monitor oscilloscope tracing of a single TV line of the image of the 100th hologram recorded and fixed. The signal has a side-to-side rolloff due to nonuniformity of the recording light beams.

side-to-side image intensity. In summary, we exclude from our definition of image noise those variations in signal amplitude that are due to fluctuations in the recording apparatus or to correctable defects such as the beam size.

The S/N ratio is defined as the ratio of the light intensity to the rms fluctuation of the light intensity. For both the TV camera tube and the photomultiplier tube the output current is proportional to the incident light intensity. The S/N ratio, SNR, expressed in dB is then:

$$\mathrm{SNR} = 20 \log(I/I_{rms}) = 20 \log(i/i_{rms}) \tag{1}$$

where I is the signal light intensity and I_{rms} is the rms fluctuation in the light intensity, i is the detector output current, i_{rms} is the rms fluctuation in the tube current. We measure the peak-to-peak noise using either of the above systems. In terms of the peak-to-peak noise intensity I_{pp} or output current i_{pp} fluctuations, the S/N ratio is

$$\begin{aligned} \mathrm{SNR} &= 20 \log(2\sqrt{2}\ \ I_S/I_{pp}) = 20 \log(2\sqrt{2}\ \ i_s/i_{pp}) \\ &= 9.03\ \mathrm{dB} + 20 \log(I_S/I_{pp}) \\ &= 9.03\ \mathrm{dB} + 20 \log(i_s/i_{pp}) \end{aligned} \tag{2}$$

III. S/N MEASUREMENTS

The purpose of this program is to measure the degradation in image quality, if any, as the number of images stored is increased. To measure this effect we recorded and fixed ten holograms of the object shown in Fig. 2 in a crystal of iron-doped $LiNbO_3$. One hundred holograms of the same object were recorded and fixed in a crystal from the same boule which had undergone the same thermal treatments. S/N measurements were made on the readout images from each of these crystals using the image slicer, scanning photomultiplier systems and the spectrum analyzer discussed above.

A. TRANSMITTED OBJECT BEAM

Recording and readout of thick phase holograms require the use of highly coherent monochromatic light. The use of coherent light, however, shows up even the smallest defects in an optical system. Imperfections in the object, imaging optics, and recording medium such as bubbles and scratches, dust on these elements and fringes from multiple reflections, produce an image replete with bullseyes, mottling, and fringes. Figure 6(a) shows an example of this effect as photographed from the Conrac monitor. For comparison purposes, Fig. 6(b) shows the same image when the object is illuminated with incoherent white light. Defects visible with monochromatic laser light are not visible with incoherent white light since the broad range of wavelengths in the source smear out diffraction patterns, multiple reflections, etc. Diffuse illumination of the object with laser light will produce an image which is free of such cosmetic defects. Such illumination, however, produces speckle noise which increases in severity as the size of the aperture of the imaging system decreases [10].

Earlier work on thin phase holograms at RCA Laboratories showed that an optimum solution to this problem exists between the extremes of diffuse illumination and single beam illumination. Gerritsen et al. [10] have shown that a two-dimensional source of illuminating beams reduces the effect of system defects significantly without introducing objectionable speckle noise. They

10. H. J. Gerritsen, W. J. Hannan, and E. G. Ramberg, Appl. Opt. 7, 2301 (1968).

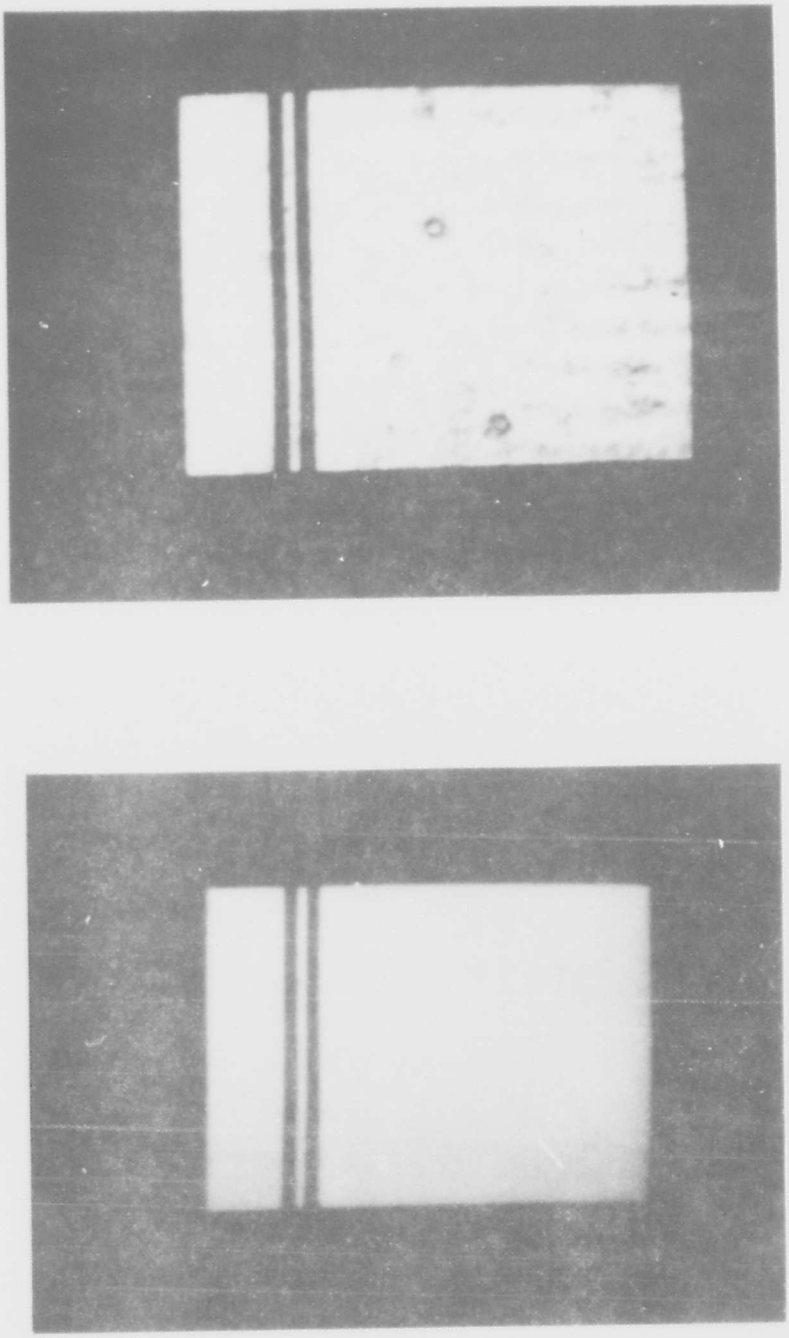

Figure 6. Television image of the object transparency (a) illuminated with a single laser beam; (b) illuminated with a tungsten filament lamp.

used a two-dimensional phase grating to generate a multiplicity of object beams of approximately equal amplitude. This arrangement produces a measure of immunity or redundancy from system defects since each of the object beams travels a different path through the optical system and records a separate subhologram with the reference beam. The S/N ratio of this multiple beam hologram is then increased over that of a subhologram by $\sim\sqrt{N_1}$ where N is the number of subholograms. The maximum amount of redundancy obtainable for a given object and recording arrangement has been analyzed by Firester et al. [11].

In our work a two-dimensional thin phase grating with 750 lines/inch spatial frequency was used to produce the multiplicity of object beams. This grating produced nine beams of approximately equal amplitude and a large number of less intense beams from the higher diffraction orders. Figure 7 shows the

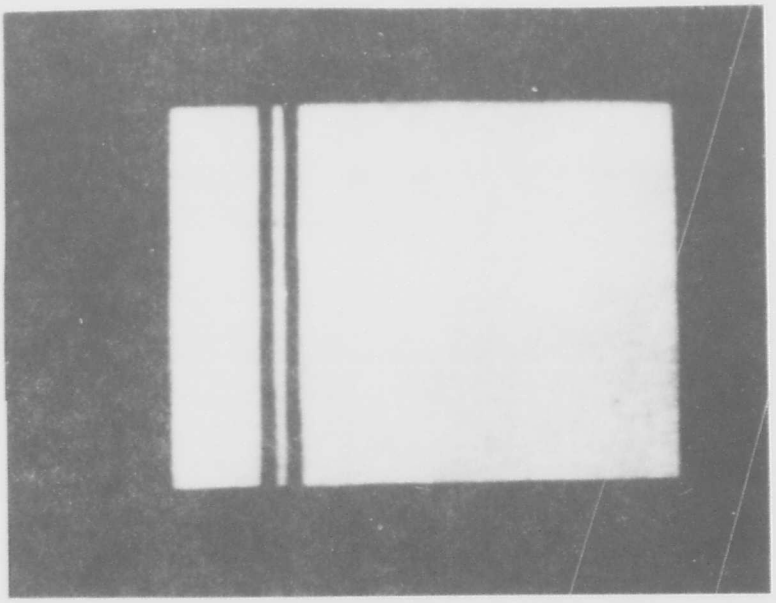

Figure 7. Television image of the object transparency illuminated with multiple laser beams.

11. A. H. Firester, E. C. Fox, T. Gayeski, W. J. Hannan, and M. Lurie, RCA Review 33, 131 (1972).

transmitted object beam with the grating in place. This is to be compared with Fig. 6(a) for a comparison of the cosmetic quality of the object with and without multiple object beam illumination.

The use of multiple object beam illumination will also superpose the spatial frequency of the source grating on the object. For a particular application the spatial frequency of the source grating must exceed the maximum spatial resolution of the display. Illumination of the 10 mm wide aperture with the 750 line/inch grating produces a pattern with a spatial frequency of 29.5/mm in the horizontal direction. For a TV system with a horizontal scan time of 53 μs, a raster width of 13.5 mm, and an optical magnification of 1.25X, this is equivalent to 6 MHz. Figure 8 is a oscilloscope trace from a

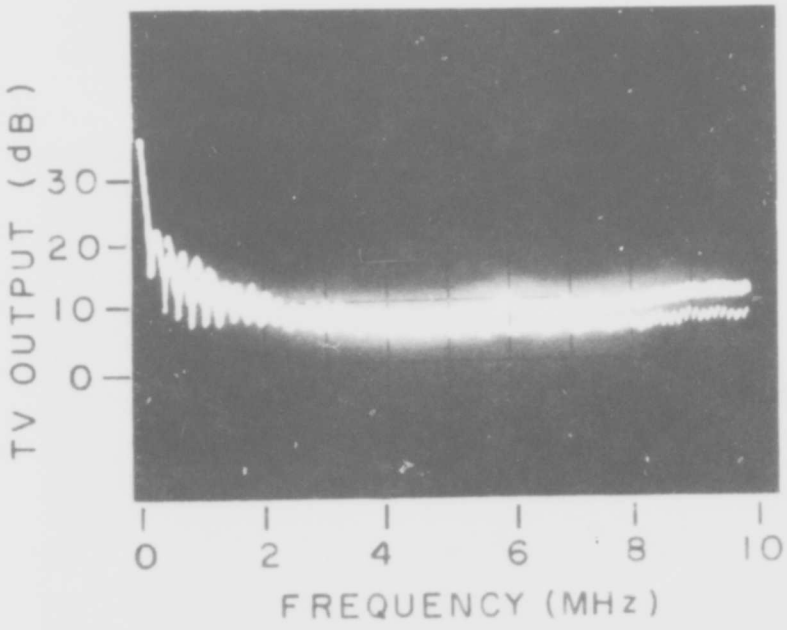

Figure 8. Spectrum analyzer tracing of the frequency spectrum of the readout image in showing 6 MHz frequency component due to the phase grating.

Hewlett-Packard 8553B spectrum analyzer showing a small peak at ∿6 MHz corresponding to the grating pattern. This is demonstrated more clearly in Fig. 9. Figure 9(a) is a photograph of the transmitted object beam after it is magnified 2.5X and displayed on the monitor. Figure 9(b) shows the corresponding trace from the spectrum analyzer. Because of the magnification of the object,

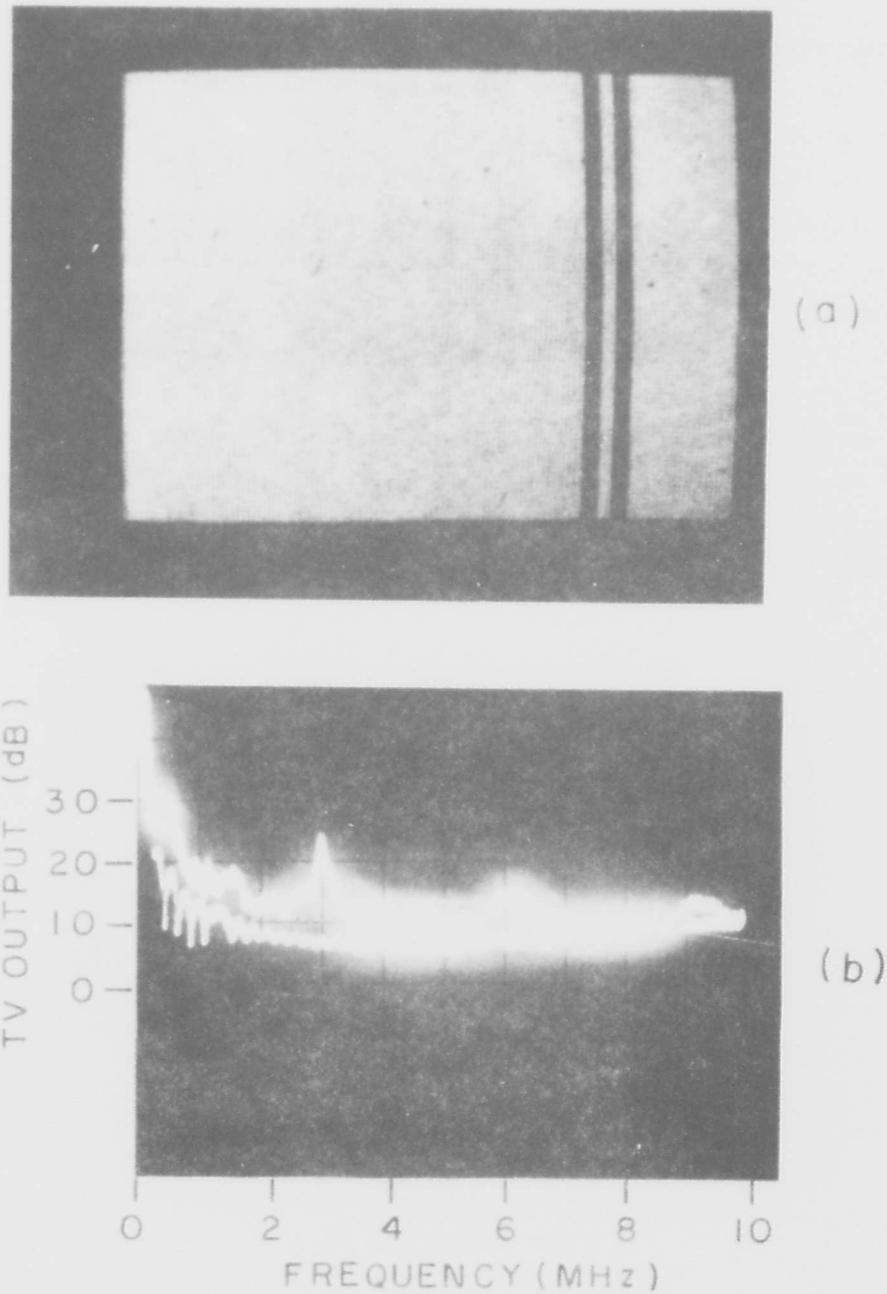

Figure 9. (a) Television image of the object transparency as in Fig. 7, but with 2.5X greater magnification in the recording optics. (b) Spectrum analyzer tracing of the frequency spectrum of the image shown in (a). The grating frequency and its harmonics are reduced by a factor of 2 corresponding to the increased system magnification.

the grating pattern is well within the bandpass of the display system and can be clearly seen. The spectrum analyzer photograph shows that the image contains a large ∿3 MHz component and harmonics corresponding to the magnification of 2.5X. The interpretation of these results will be discussed in detail below.

Using the image slicer and TV system the S/N ratio of the transmitted object beam was measured to be 29-31 dB using the grating and optical system described above.

B. READOUT IMAGES

1. Crosstalk

Ten and one hundred holograms were recorded and fixed using the write-while-hot technique in 0.4-cm-thick crystals. The holograms were spaced 0.2° apart. Hologram crosstalk was measured by leaving one hologram position blank between the 49th and 50th holograms and measuring the light intensity scattered from the crystal at the angle where the missing hologram was located. Scattered light due to surface and bulk defects was estimated from the scattered light intensity at angles beyond the range over which the holograms were recorded. From these measurements the rms crosstalk noise was estimated to be ∿−51 dB down from the peak image intensity. This is in good agreement with a theoretical estimate of -54 dB obtained assuming incoherent addition of crosstalk intensities [12]. The magnitude of the scattered light due to defects and optical damage during recording was estimated to be of the same magnitude ($\lesssim$ -51 dB).

2. Hologram Amplitude

As noted above, the S/N measurements do not include the variations in peak signal intensity from hologram to hologram within a sequence of recorded holograms. In our work we found that in two recordings of 10 holograms, the average signal/peak-to-peak fluctuation was 2. For 100 holograms, the average signal/peak-to-peak fluctuation was ∿1.5. The fluctuations in both cases are random, due most likely to recording system perturbations.

12. W. J. Burke, Monthly Report, Contract No. N00014-75-C-0590, October 10, 1975.

The $1/N^2$ decrease in S/N ratio, where N is the number of holograms recorded observed by Zech [13], is not observed in this experiment since this decrease is due to a decrease in the diffracted signal power of successively recorded holograms. We do not observe this effect because in the recording procedure we compensate with variable exposure times.

3. S/N Measurements with the Image Slicer

Figure 10 shows photographs taken off the TV monitor of (a) 1st, (b) 50th, and (c) 100th holograms recorded and fixed, and read out with no bandpass filter in the system. As displayed on the monitor and observed visually, there does not appear to be any significant variation in image quality.

The measured S/N ratio obtained using the image slicer system is shown in Fig. 11. Shown in this figure are the results for one recording of ten holograms and two different recordings of one hundred holograms with either no filter or a 5 MHz low-pass filter in the system. The two separate recordings of 100 holograms produced a mean S/N ratio of 27.4 and 24 dB, respectively, for the case where the 5 MHz filter was present in the system. With no filter in the line, the mean S/N ratio for the second recording dropped from 24 to 22.5 dB. The results for 100 holograms show what appears to be only a slight ($\sim$2 dB) degradation in S/N ratio with increasing hologram number.

The measurements on the 10 holograms and those on the first run of 100 holograms were made at the same time while the second run of 100 holograms was made at a later date on the same crystal. The mean S/N ratio for these two runs differs by approximately two standard deviations. It is therefore likely that this difference in the mean SNR is due to a change in the recording optics or in the measurement apparatus. For the case of the 10 holograms and the first run of 100 holograms, a statistical analysis of the results shown in Fig. 11 indicates that there is $\sim$30% probability that there is no difference in the S/N ratio between recording 10 and 100 holograms.

4. S/N Measurement with Scanning Photomultiplier

The S/N ratio of the readout hologram was measured directly using a photomultiplier to scan a line across the readout image. The scanning system and

13. R. G. Zech, Ph.D. Thesis, University of Michigan, 1974.

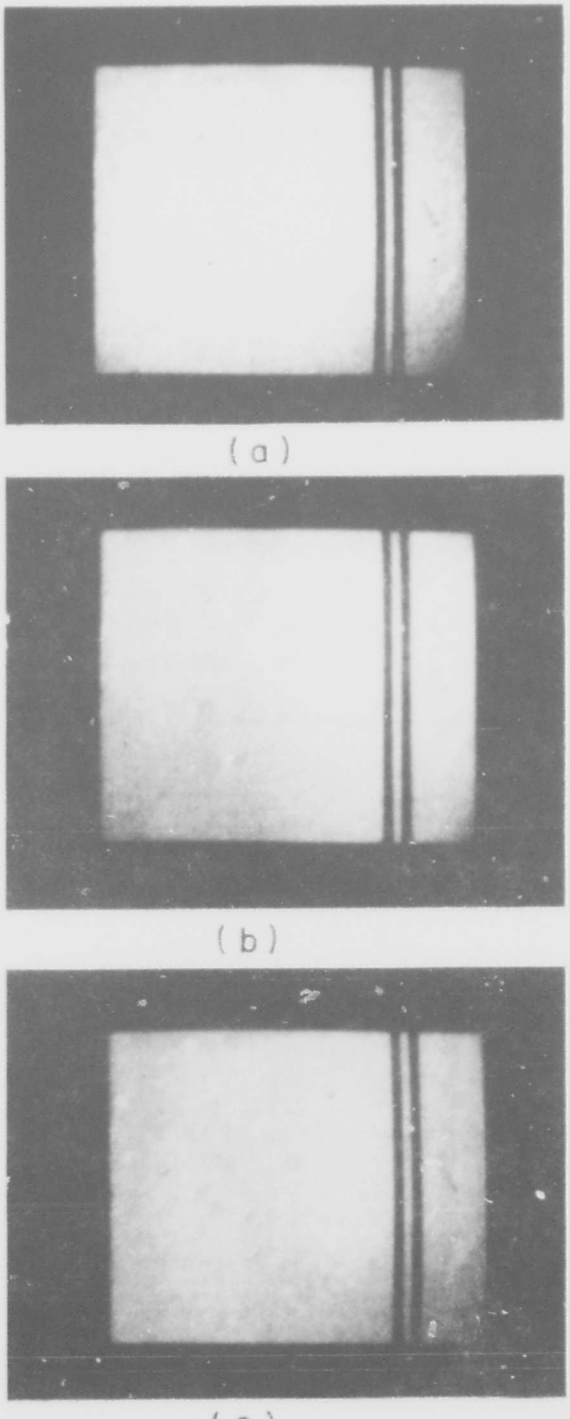

Figure 10. Television image of the (a) 1st; (b) 50th, and (c) 100th hologram recorded and fixed.

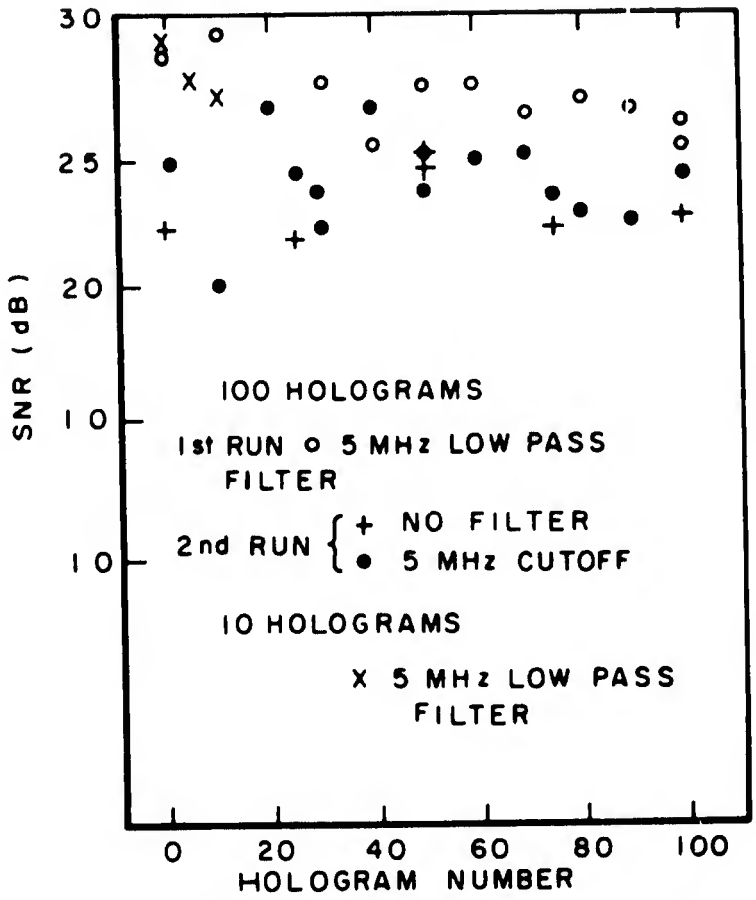

Figure 11. S/N ratio as a function of hologram number measured with the image slicer.

aperture were discussed above. For these measurements the image was magnified by a factor of eight as compared to that used for the noise measurements made with the TV system. This was done to increase the spatial resolution of the scanning aperture.

Figure 12 shows the measured S/N ratio as a function of spatial frequency in the enlarged image of a readout hologram. Also shown is the S/N ratio for the transmitted object beam measured in the same way. In each case, the S/N ratio decreases with increasing spatial frequency until it saturates at a level of 9 dB. This saturation is an artifact of the experiment in that once the signal/peak-to-peak noise reaches one (9 dB rms) we cannot measure a further increase, if any, in the noise.

The results shown in Fig. 12 are the signal/integrated noise ratio up to the cutoff of the low-pass filter which the scanning aperture forms. The

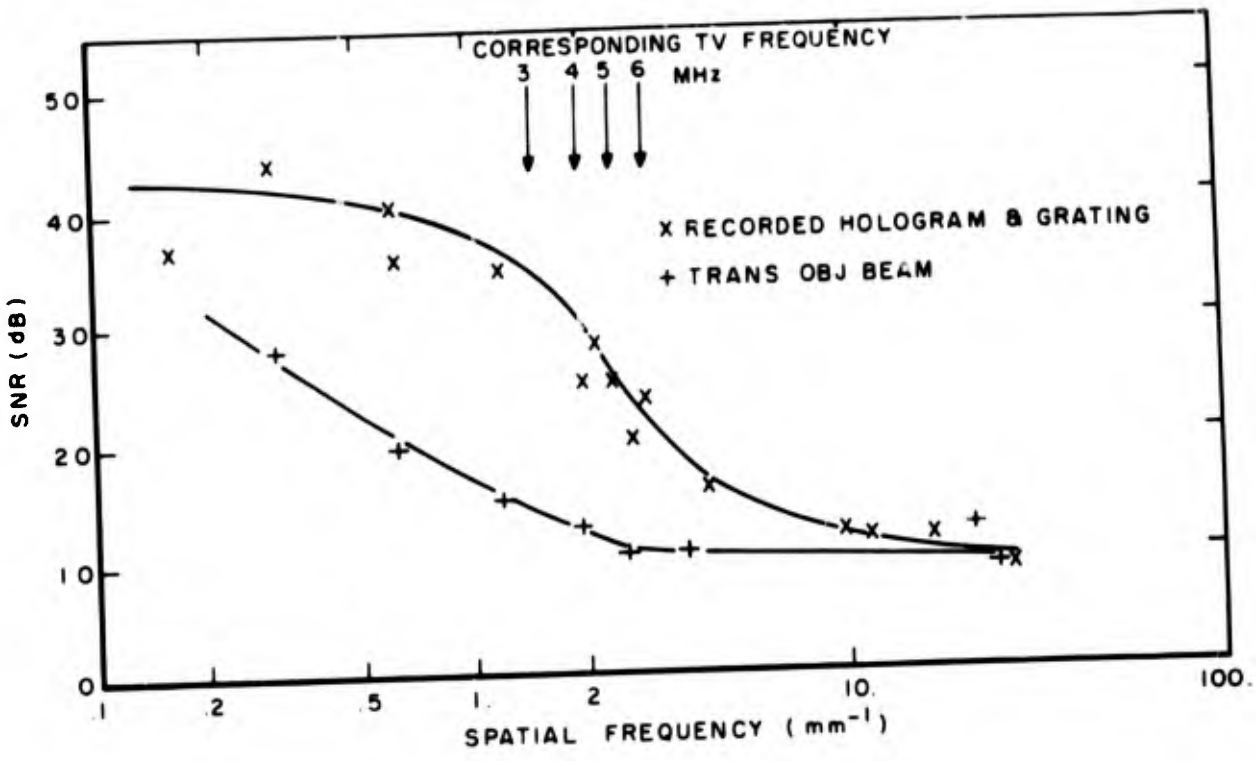

Figure 12. S/N ratio as a function of spatial frequency of the image readout from a recorded and fixed multibeam hologram measured with the scanning photomultiplier and of the object transparency illuminated with a single laser beam. The optical magnification is 8X that in Fig. 11.

signal itself has an approximately dc component (a white field) and a small 0.53 mm^{-1} component due to the slits. The decrease in S/N ratio comes about from the cumulative increase in the total noise as the bandwidth of the low-pass filter increases. The S/N ratio for the transmitted object beam decreases rapidly at low spatial frequency due to the low frequency noise contribution from cosmetic defects. In the case of the recorded multiple-beam hologram, the S/N ratio remains high over this frequency range, and then decreases as the bandpass overlaps the spatial frequency of the grating.

This measurement of the noise in the readout image is the same as that made with the image slicer and monitor in that the integrated noise up to the filter cutoff or system response cutoff, whichever is lower, is measured. The results presented here are consistent with those measured with the TV system within the range of response of the TV system. At the spatial frequency equivalent to 5 MHz in the TV experiment, the S/N ratio is essentially the same

in the two cases. With the scanner, however, it is possible to extend the range of measurements significantly further in frequency.

5. Noise Measurements with a Spectrum Analyzer

In these measurements, the image was magnified by a factor of 2.5X. The image was detected with the GPL1000 camera and its frequency spectrum measured with the HP8553B spectrum analyzer.

Figures 13(a) and (b) show oscilloscope traces for hologram number 1 of 100 over the frequency range from 0 to 5 MHz and 0 to 10 MHz, respectively. Also shown in each photograph is the baseline signal when the input light to the camera was blocked. The difference between the two traces in each photograph is the output of the TV camera as a function of frequency due to the image. The peak at 3 MHz in Fig. 13(a) and the peaks at 3, 6, and 9 MHz in Fig. 13(b) are the imaged grating fundamental frequency of 3 MHz and its harmonics as discussed above in reference to the transmitted object beam. Figure 14 shows an oscilloscope trace for the 100th hologram over the frequency range from 0 to 5 MHz. Comparison of Fig. 14 with Fig. 13(a) shows that no significant difference exists between TV output signal for the two cases. This is quite remarkable. This observation is also in agreement with the results obtained with the image slicer with no significant difference between holograms 1 and 100.

Figures 15(a) and (b) show the spectrum analyzer traces for the transmitted object without the phase-grating over the frequency range 0 to 5 MHz and 0 to 10 MHz, respectively. In these photographs the peaks at 3 MHz and its harmonics are missing since the phase-grating was not used to illuminate the object. Comparing Fig. 15(a) and (b) with Fig. 13(a) and (b) and Fig. 14, the difference between the TV output due to the image and the baseline is larger at low frequencies (3 MHz) for the transmitted object beam than for holograms recorded with multiple object beam illumination.

The object used in these tests, as shown in Fig. 2, is a white field which covers ∿40% of the transparency width with two slits in the field. The white field will produce a spatial frequency of ∿1.5 kHz at this magnification. The two slits will produce a spatial frequency of ∿0.5 MHz plus harmonics. Thus, on the frequency scale shown here, the signal field is essentially dc, while the slits will contribute a small component at ∿0.5 MHz. The

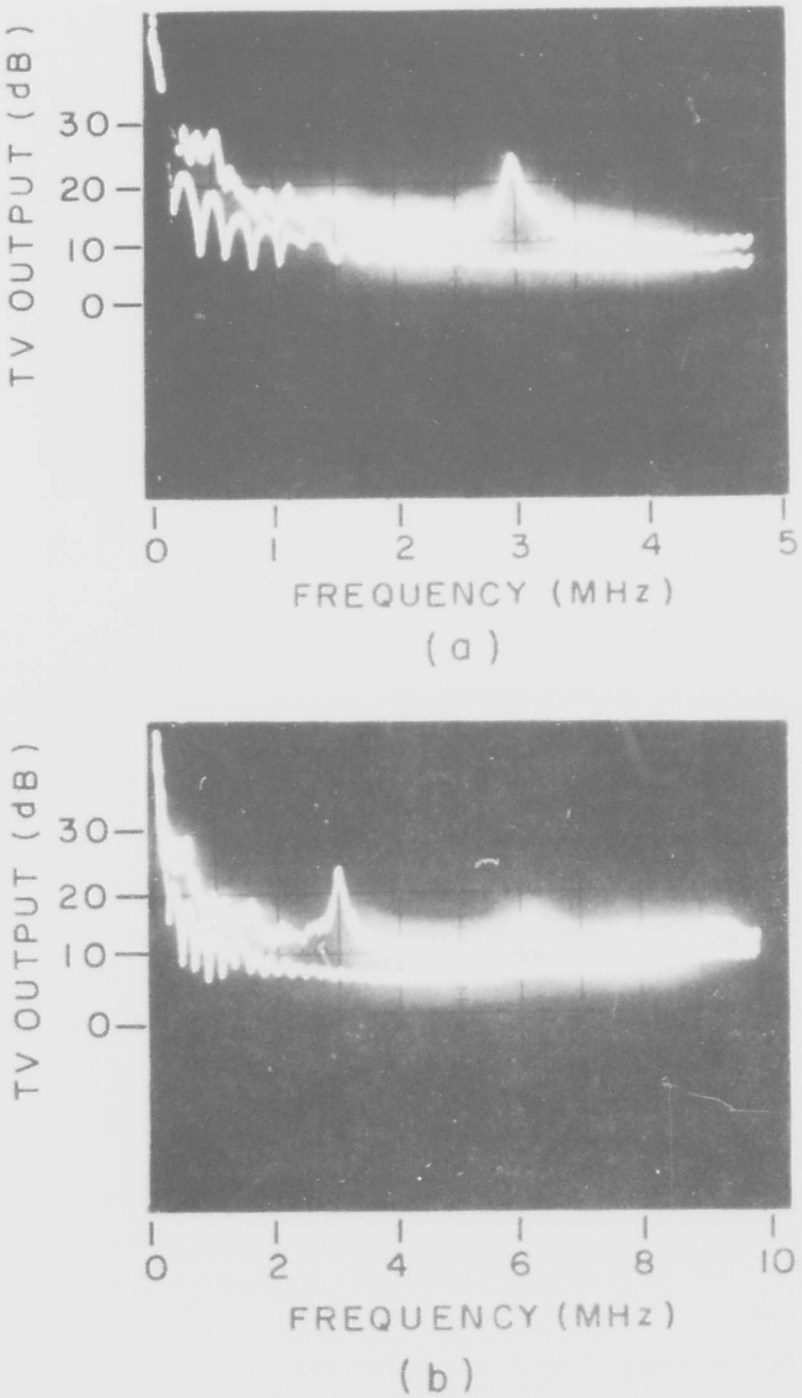

Figure 13. Spectrum analyzer tracing at an optical magnification 2X that of Fig. 11 of the readout image from the 1st of 100 holograms. (a) over the 0 to 5 MHz frequency range; (b) over the 0 to 10 MHz frequency range.

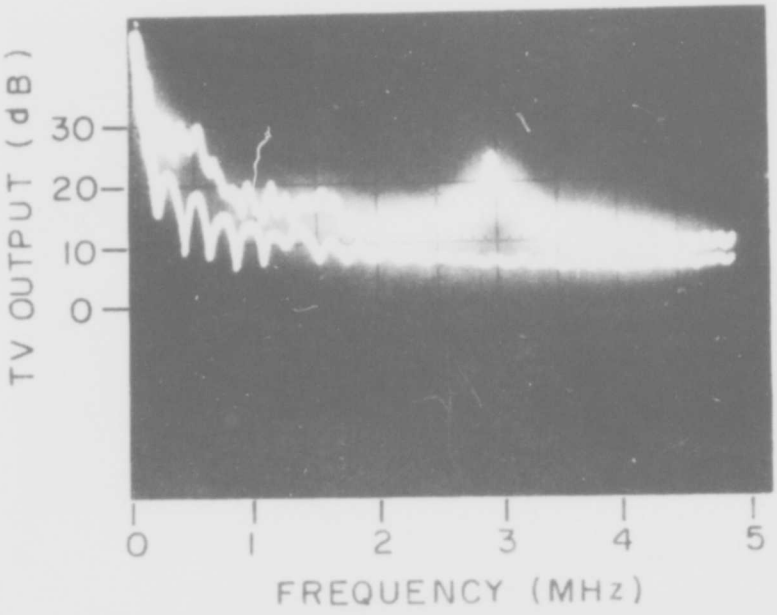

Figure 14. Spectrum analyzer tracing as in Fig. 13 of the readout image from the 100th hologram over the 0 to 5 MHz frequency range.

remainder of the signal observed is then due to noise in the image. The spectrum analyzer output signals for hologram number 1 and for the transmitted object beam with single beam illumination are plotted in Fig. 16. [The spatial frequency scale shown in Fig. 16 is four times that in Fig. 12 due to the differing magnifications.] Figure 16 is the derivative of the results shown in Fig. 12 because here we are measuring the output of the camera tube over a narrow passband at the spatial frequency of interest, while Fig. 12 shows the $\sim$dc signal/integrated noise ratio.

The results presented in Fig. 16 show that the noise decreases with increasing spatial frequency over the range of frequencies measured here. The noise is primarily low frequency in nature and is associated with the cosmetic defects (dust, scratches, etc.) as shown in Fig. 6(a). The primary noise source in the readout image at high spatial frequency is the redundancy device itself.

As discussed above, the use of a redundance device reduces the noise in the readout image by $\sim\sqrt{N}$, where N is the number of subholograms recorded

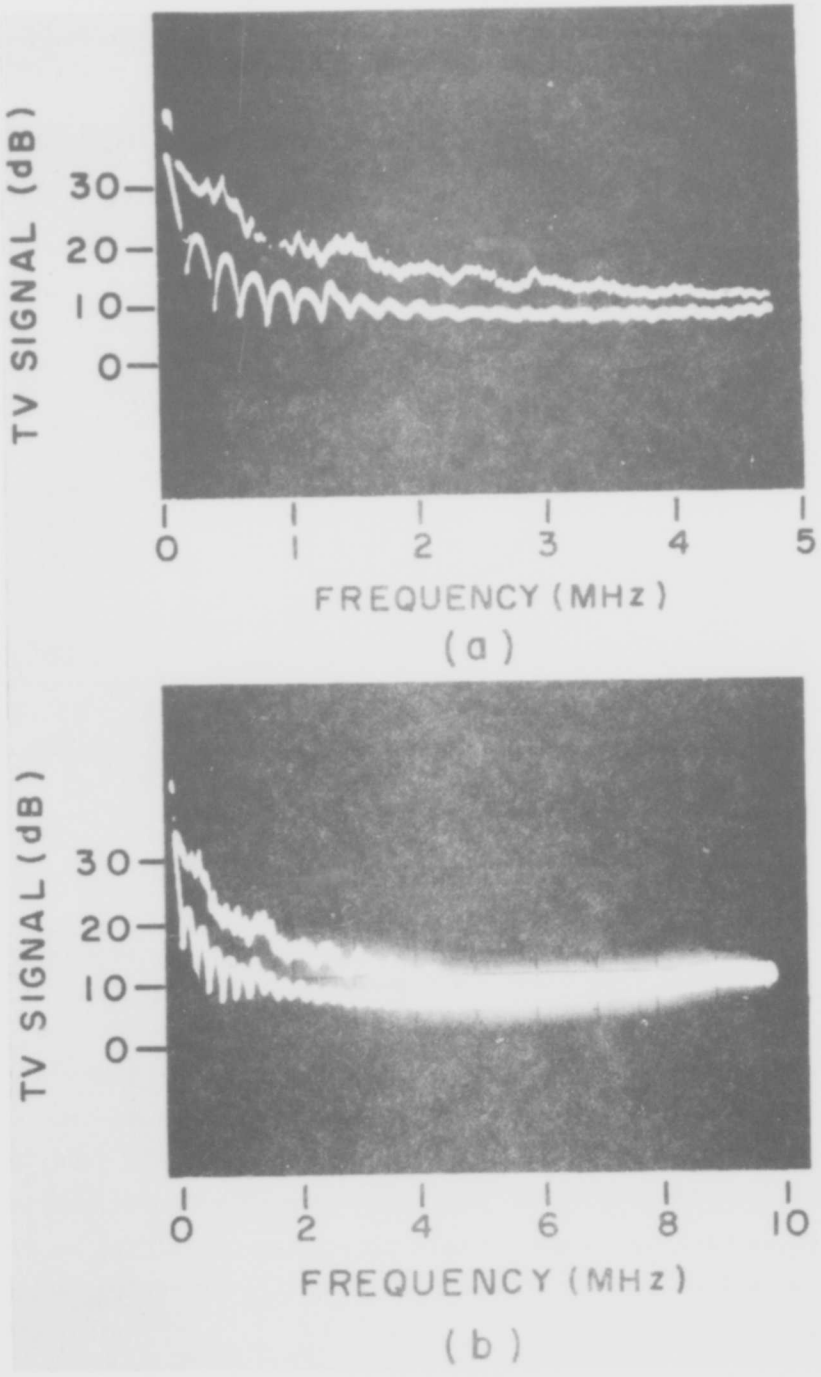

Figure 15. Spectrum analyzer tracing of the object transparency illuminated with a single laser beam. (a) over the frequency range 0 to 5 MHz; (b) 0 to 10 MHz.

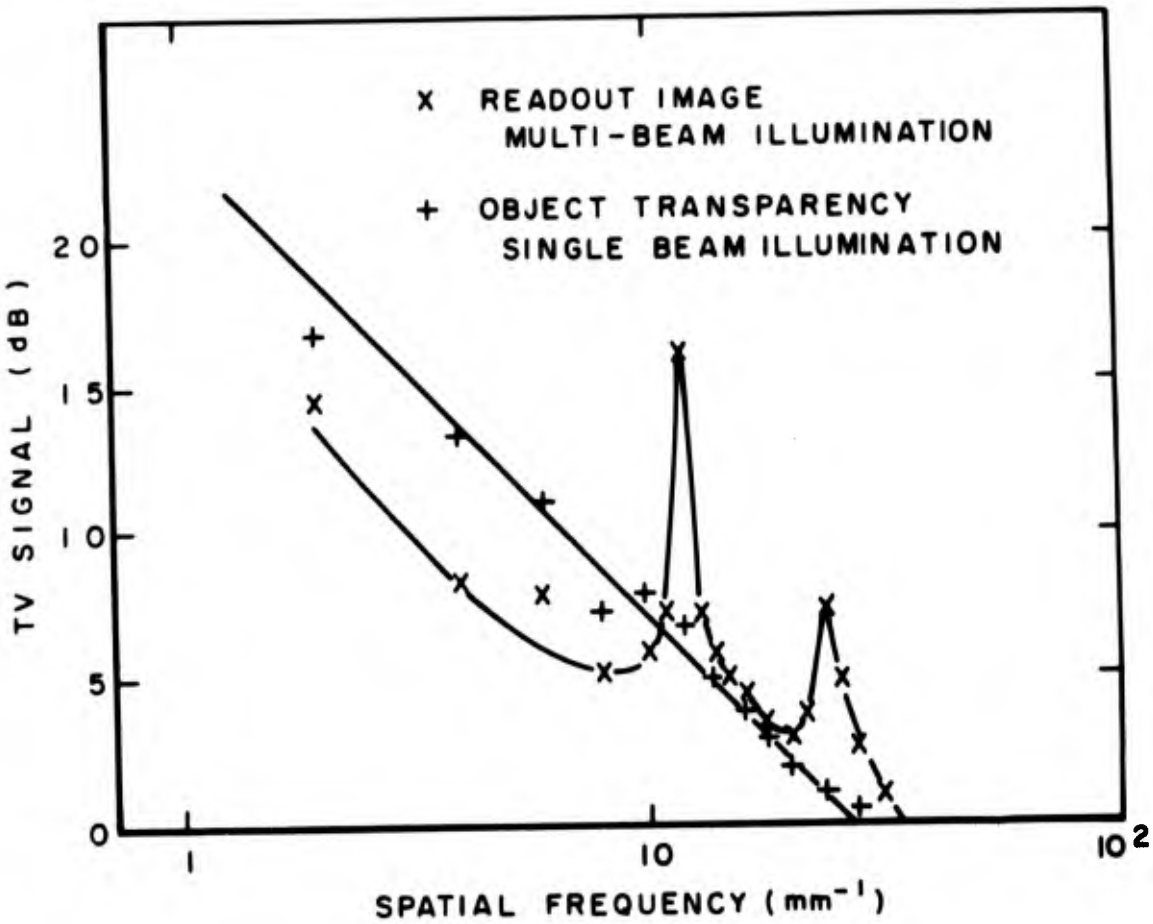

Figure 16. Data from Fig. 13 and Fig. 15 plotted as a function of spatial frequency. The optical magnification is 1/4 that shown in Fig. 12.

using the multiple beam illumination. From Fig. 16 we see that below the grating frequency, the noise in a given frequency range is reduced by ∿6 dB. This is equivalent to $\sqrt{N} = 2$, or that four subholograms were recorded rather than the 9 expected for this grating. This difference is probably due to a combination of aperturing in the optical system and nonuniform overlap of the recording beams which leads to a reduction in the contribution of some of the subholograms.

IV. SUMMARY AND CONCLUSIONS

From the measurements with the TV system and the spectrum analyzer presented here, there does not appear to be any significant degradation in the S/N ratio in the readout image with increasing numbers of holograms. These measurements were limited primarily by the large amount of noise in our recording apparatus. The primary source of noise in these recordings was scattering from defects and multiple reflections in the optics. Crosstalk and light-induced defect scattering were much smaller (-25 to -30 dB) than the contribution from the optical system.

The results presented show that the recording of multiple object beam holograms can considerably reduce the low spatial frequency noise due to these defects. The price paid for this improvement is the introduction of a noise source at the fundamental frequency and harmonics of the redundancy device. This is most clearly seen from Fig. 12 and Fig. 16. From these figures we see that the signal/integrated noise is high ($\sim$35 to 40 dB) at frequencies less than 14 mm^{-1} in the object transparency. The decrease at higher spatial frequencies is due to the presence of the grating as a noise source. For objects with spatial frequencies $\leq 14mm^{-1}$, improved optics and greater redundancy can lead to significant further improvements in the S/N ratio.

Figure 16 shows that the scattering noise decreases with increasing spatial frequency. Therefore, for objects containing primarily high spatial frequencies, scattering noise is not as important. Since this is precisely the range in which the redundancy device itself is the dominant noise source, such devices should not be used for objects containing primarily high spatial frequency. For this case low frequency spatial filtering and improved optics would be the preferable approach.

REFERENCES

1. J. J. Amodei, W. Phillips, and D. L. Staebler, IEEE, J. Quantum Electron. QE-7, 63 (1971).
2. G. E. Peterson, A. M. Glass, and T. J. Negran, Appl. Phys. Lett. 19, 130 (1971).
3. F. S. Chen, J. T. LaMacchia, and D. B. Frazer, Appl. Phys. Lett. 13, 233 (1968).
4. D. L. Staebler and J. J. Amodei, J. Appl. Phys. 43, 1042 (1972).
5. J. J. Amodei, and D. L. Staebler, Appl. Phys. Lett. 18, 540 (1971).
6. W. J. Burke, W. Phillips, D. L. Staebler, and B. F. Williams, *Materials for Phase Holographic Storage*, Final Report, Contract No. N00019-74-C-0312, April 1975.
7. G. A. Alphonse and W. Phillips, *Read-Write Holographic Memory with Iron-Doped $LiNbO_3$*, Final Report, Contract No. NAS8-26808, May 1975.
8. D. L. Staebler, W. Phillips, W. Burke, and B. W. Faughnan, *Materials for Phase Holographic Storage*, Final Report, Contract No. N00019-73-C-0273, February 1974.
9. W. J. Burke and D. L. Staebler, *Volume Hologram Material Device Feasibility for Map Display Applications*, Final Report, Contract No. N62269-72-C-0793, June 1973.
10. H. J. Gerritsen, W. J. Hannan, and E. G. Ramberg, Appl. Opt. 7, 2301 (1968).
11. A. H. Firester, E. C. Fox, T. Gayeski, W. J. Hannan, and M. Lurie, RCA Review 33, 131 (1972).
12. W. J. Burke, Monthly Report, Contract No. N00014-75-C-0590, October 10, 1975.
13. R. G. Zech, Ph.D. Thesis, Univ. of Michigan, 1974.